Journal of Sedimentary Environments
https://doi.org/10.1007/s43217-024-00200-x

RESEARCH

Provenance signature and tectonic setting of the Pliocene Tipam Sandstone Formation from the Chittagong Tripura Fold Belt of the Bengal Basin

Abu Sadat Md. Sayem[1] · Papiya Mondal[1] · Md. Sha Alam[2] · Rashed Abdullah[1] · Julleh Jalalur Rahman[1] · Rumana Yeasmin[1]

Received: 22 May 2024 / Revised: 25 July 2024 / Accepted: 28 July 2024

Abstract
The Pliocene Tipam Sandstone Formation is widely exposed in various structures of the Chittagong Tripura Fold Belt in the Bengal Basin. Petrography and major element geochemistry of sandstones from this formation have been examined to infer their provenance signature and tectonic setting. The average modal ($Q_{77}F_{11}L_{12}$) composition and geochemical results reveal that the Tipam sandstones are classified as litharenite to sublitharenite and lithic subarkose. The higher ICV (> 1) values and the negative correlation between SiO_2/Al_2O_3 and total quartz (Qt) indicate that the investigated sandstones are compositionally immature. The petrographic and geochemical provenance discriminant diagrams suggest a recycled sedimentary provenance, with sediments derived predominantly from felsic igneous sources. The weathering indices, including the CIA (Chemical Index of Alteration), PIA (Plagioclase Index of Alteration), CIW (Chemical Index of Weathering), and A–CN–K [$Al_2O_3-(CaO^*+Na_2O)-K_2O$], (A–K)–C–N [$(Al_2O_3–K_2O)-CaO^*-Na_2O$)], A–CNK–FM [$Al_2O_3$–($CaO^*+Na_2O+K_2O$)−($Fe_2O_3+MnO$)], and MFW [Mafic–Felsic–Weathering] models, indicate a weak to moderate degree of chemical weathering. The paleoclimate model reflects a sub-humid climate condition in the source area. The results imply that the Tipam Sandstone Formation accumulated in an active continental margin context, with the majority of sediments sourced from the Lesser Himalayan Sequence and a smaller portion from the Higher Himalayan Crystalline Sequence, Sub-Himalaya, and Indo-Burma Ranges during the Pliocene.

Keywords Petrography · Geochemistry · Provenance · Chemical weathering · Tectonic setting · Bengal Basin

1 Introduction

Provenance studies of sandstones are crucial for understanding the source rock complex, chemical weathering, and tectonic setting. The detrital modes and geochemistry of terrigenous sediments are widely used to constrain the provenance of clastic rocks (Dickinson & Suczek, 1979; Ingersoll & Suczek, 1979; Dickinson, 1985; Roser & Korsch, 1986; Suttner & Dutta, 1986; Hayashi et al., 1997; Armstrong-Altrin et al., 2017, 2021; He et al., 2019; Noa Tang et al., 2020; Sayem et al., 2023). In addition, mineralogical and major element abundances of siliciclastic rocks were utilized to decipher the tectonic settings of the source terrain (Ingersoll & Suczek, 1979; Murphy, 2000; Roser & Korsch, 1986; Verma & Armstrong-Altrin, 2013). Furthermore, sediments originate from parent rocks through weathering processes, making them suitable candidates for provenance evaluation (Nesbitt & Young, 1982, 1984; Harnois, 1988; Wronkiewicz & Condie, 1987; Fedo et al., 1995; Cullers, 2000; Singh, 2010; Sayem et al., 2018).

The Pliocene Tipam Sandstone Formation is extensively exposed in the Chittagong Tripura Fold Belt (CTFB) of the Bengal Basin (Fig. 1c). Previous sedimentological studies from the CTFB have mainly focused on the underlying Miocene Surma Group sediments and the overlying Dupitila Formation (Alam et al., 2003; Dina et al., 2016;

Communicated by M. V. Alves Martins.

✉ Abu Sadat Md. Sayem
sayem8282@juniv.edu

[1] Department of Geological Sciences, Jahangirnagar University, Savar, Dhaka 1342, Bangladesh

[2] Institute of Mining, Mineralogy and Metallurgy (IMMM), Bangladesh Council for Scientific and Industrial Research (BCSIR), Joypurhat, Bangladesh

Published online: 03 August 2024

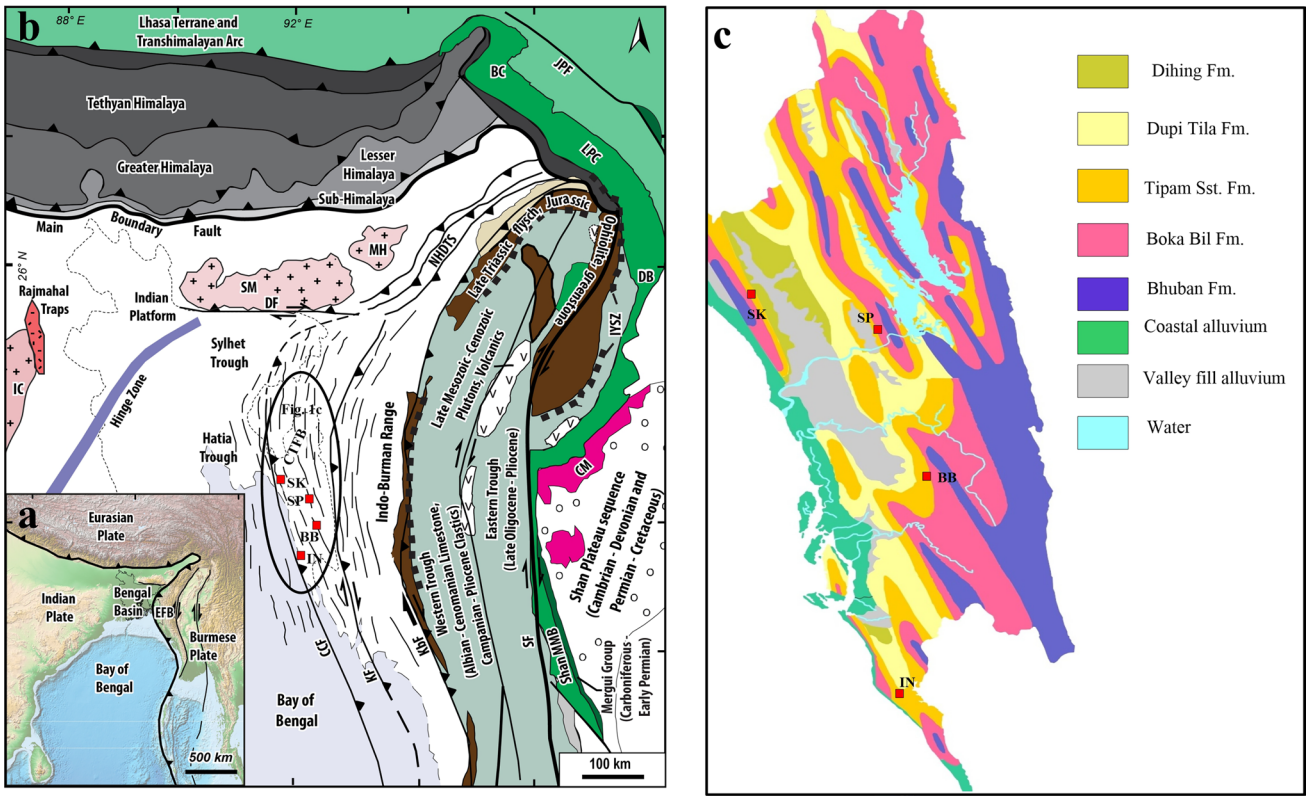

Fig. 1 **a** Location map of the Bengal Basin and its regional setting: **b** tectonic elements of the Bengal Basin and its surrounding areas (modified after Johnson & Alam, 1991; Sayem et al., 2022); **c** traditional stratigraphy of the CTFB [the red squares indicate the sampling structures; where SK, Sitakund Anticline; SP, Sitapahar; Anticline; BB, Bandarban Anticline; IN, Inani Anticline]

Rahman et al., 2014a, 2014b, 2020; Sayem & Rahman, 2012; Sayem et al., 2022; Yang et al., 2019, 2020; Yeasmin et al., 2024). In contrast, little is known about the Pliocene Tipam Sandstone Formation (Rahman et al., 2020). So far, no provenance studies have been conducted that integrate its petrography, geochemistry, and tectonic context. However, the origin of the CTFB sediments remains unclear. Numerous studies have indicated that the underlying Miocene Surma Group sediments were mainly derived from Himalayan Orogen (Najman et al., 2008; Rahman & Faulp, 2003; Rahman et al., 2014a, 2014b; Yang et al., 2019). In contrast to the Surma Group sediments, the younger zircon ages (< 200 ma) identified in the Tipam Sandstone Formation (Najman et al., 2012; Rahman et al., 2020) suggest a secondary detrital input from the Indo-Burma Ranges (IBR). Thus, the mixing of IBR and Burma magmatic inputs with Himalayan-originated detritus in the CTFB is still debated. The main purpose of this study is to investigate detailed petrography and major element geochemistry of the Pliocene Tipam Sandstone Formation from the Chittagong Tripura Fold Belt of the Bengal Basin. The major objectives are to infer the provenance, the intensity of chemical weathering, and tectonic environments of the Bengal Basin during the Pliocene.

2 General geology

The geological evolution of the Bengal Basin (Fig. 1a) is intricately linked to the initial collision between the Indian and Eurasian plates, followed by subsequent interaction with the Burmese plate. Tectonically, the Bengal Basin is divided into three geotectonic regions, namely, the Indian Platform to the northwest; the Sylhet Trough and the Hatia Trough in the Central Deep Basin; and the Chittagong Tripura Fold Belt (also known as the Eastern Fold Belt, EFB) to the southeast (Alam et al., 2003) (Fig. 1b). The structural configuration of the Bengal Basin commenced with the rifting of the Gondwanaland during the Early Cretaceous period (Abdullah et al., 2022; Shamsuddin & Abdullah, 1997). The ongoing northward movement and eventual collision between the Indian and Eurasian plates led to the east–west oriented Himalayan Mountain ranges (Curray, 1991) during the Eocene. These orogenic processes were the primary contributors of sediments, leading to sedimentation in both the Indian Platform and the Central deep basinal part of the Bengal Basin (Abdullah et al., 2022; Alam et al., 2003; Najman et al., 2008, 2012). During the Oligocene–Miocene, the oblique collision between

the Indian and the Burmese plates resulting the NNW-SSE trending Indo-Burman Ranges (Alam et al., 2003; Davies et al., 2003) to the east. In the Miocene, the Bengal Basin transformed into a remnant ocean basin due to the ongoing subduction of the Indian plate under the Burmese plate, and the CTFB became the major sediment depocenter (Alam et al., 2003). During the Mid-Pliocene, a fluvio-deltaic environment emerged as the ultimate marine regression, causing the sediment depocenter to relocate south of the basin (Alam et al., 2003; Davies et al., 2003; Abdullah et al., 2021a). By the Early-Middle Pleistocene, the persistent subduction of the Indian plate caused the compression of sediments resulting in their upliftment to form NNW-SSE trending anticlines within the CTFB (Abdullah et al.,).

Tectonically, the CTFB represents the western flank of the Indo-Burman Ranges and is separated from the eastern flank by the Kaladan Fault (Fig. 1b). The western boundary of the CTFB is marked by the Pleistocene Lalmai Hills (Abdullah et al., 2021b), while the Dauki Fault defines its northern limit. The CTFB in the Bengal Basin (Fig. 1b) contains an extremely thick (~ 3500 m) accumulation of Neogene clastic deposits (Alam et al., 2003; Davies et al., 2003), with sediments derived from the Indo-Burman Ranges and the eastern Himalayas (Reimann, 1993; Alam et al., 2003; Najman et al., 2008; Rahman et al., 2020; Yang et al., 2020. Because of the absence of a distinctive marker horizon and limited biostratigraphic zonation, the age correlation of these sediments remains unknown. The conventional stratigraphic scheme followed for the CTFB rock successions is illustrated in Fig. 1c and summarized in Table 1. The middle Miocene Bhuban Formation is the oldest rock unit in the CTFB followed by the Late Miocene Bokabil Formation (Reimann, 1993; Alam et al., 2003). The studied Tipam Group unconformably overlays the Bokabil Formation. The sedimentary process of this Group was associated with a marine regression (Davies et al., 2003; Gani & Alam, 2003). The Tipam group is divided into two formations, namely the Tipam Sandstone Formation and the Girujan Clay Formation. The Tipam Sandstone Formation is characterized by a yellowish grey to yellowish brown color, fine- to medium-grained, parallel bedded, large-scale trough, and planar cross-bedded sandstones (Fig. 2a–d). The mottled nature Girujan Clay Formation is poorly exposed in the CTFB. A braided fluvial environment has been interpreted for the Tipam Sandstone Formation (Alam et al., 2003; Davies et al., 2003; Gani & Alam, 2003). The Tipam Group is unconformably overlain by the Plio-Pleistocene Dupitila Sandstone Formation in the CTFB.

3 Methodology

The sandstone samples were collected from the Tipam Sandstone Formation exposed in Bandarban anticline of the CTFB (Fig. 1b, c). The bulk samples were air-dried at room temperature prior to laboratory analysis. They were then treated with Canada Balsam to harden them, as most of the Tipam sandstones were moderately compacted. The rock samples were cut into smaller chips and polished with grinding powder of different sizes until they reached the desired thickness of 0.03 mm. Finally, the polished chips were mounted on glass slides using Araldite and covered with thin glass to avoid dust contamination. The modal composition of 20 samples was analyzed using a MEIJI ML 9000 polarizing microscope. At least 400 grains from each sample were examined using the point-counting method. The mineralogical compositions of the Tipam sandstones are listed in Table 2.

On the other hand, 22 sandstone samples were chosen for geochemical analysis using X-ray fluorescence (XRF). The samples were crushed and powdered with a planetary ball mill (PM-200, Retsch, Germany) for 20 min and then treated with 30% HCl and 10% H_2O_2 to remove organic matter. The

Table 1 Stratigraphic succession of the CTFB (modified *after* Johnson & Alam, 1991; Reimann, 1993; Alam et al., 2003; Davies et al., 2003; Gani & Alam, 2003)

Age	Group	Formation	Lithology	Depo. Envir	Major Tectonic events
Pleistocene	Dupitila	Dupitila Sandstone	Variegated color, medium to coarse-grained, poorly consolidated sandstone	Fluvial	Overthrusting of the Shillong Plateau, and rapid exhumation of the Himalayan, and Indo-Burman
liocene	Tipam	Girujan Clay	Mottled clay, with plant debris		
		Tipam Sandstone	Dark gray to yellowish brown color, fine- to medium-grained sandstone		
Miocene	Surma	Bokabil	Silty shale, fine sandstone, and calcareous sandstone	Deltaic	The collision between the Indian, Eurasian, and Burmese Plate
		Bhuban	Silty shale, sandy shale, siltstone, mudstone, and fine sandstone	Shallow Marine	
Base not found					

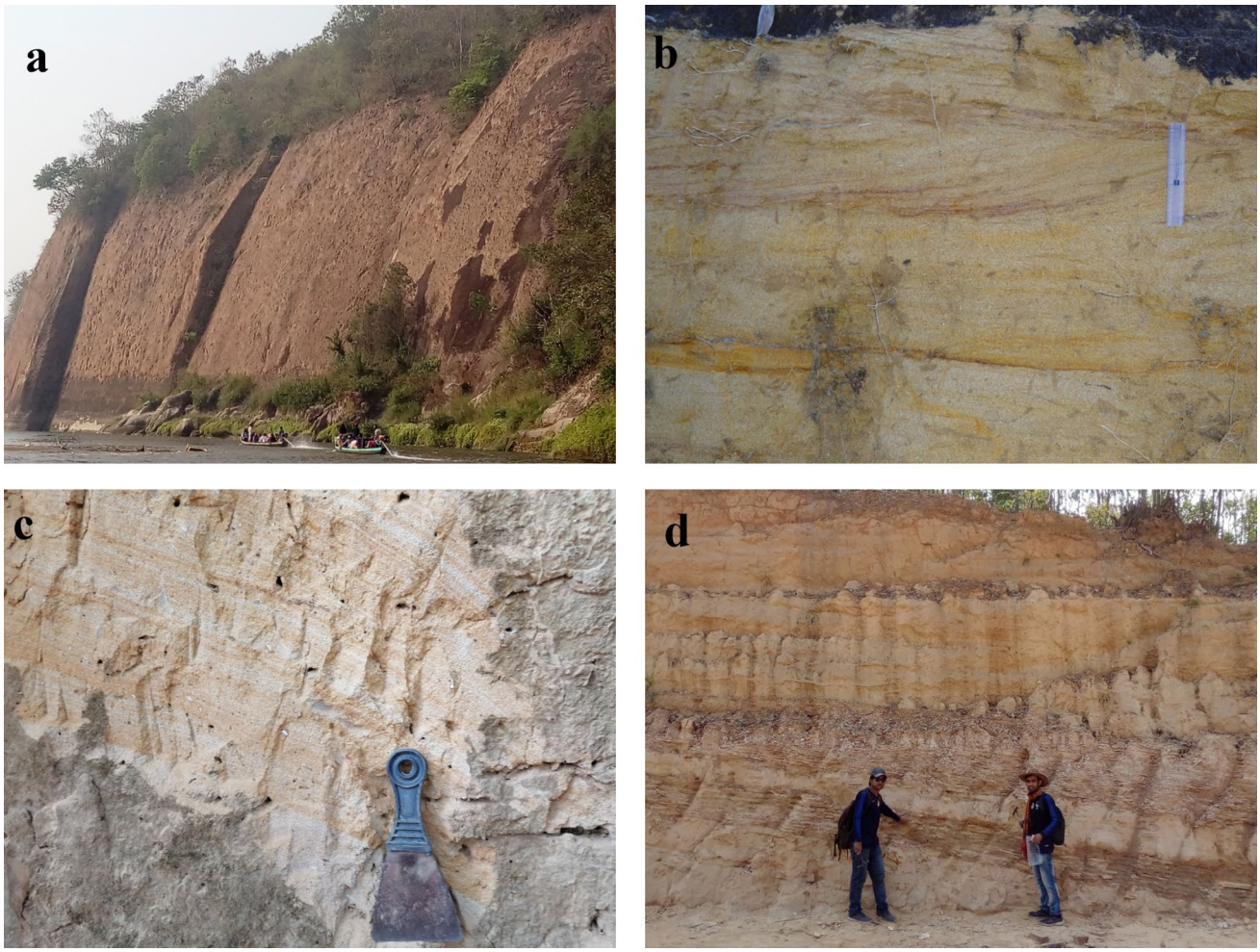

Fig. 2 Outcrop photographs of the Tipam Sandstone Formation from Bandarban Anticline (**a**, **d**), Sitapahar Anticline (**b**) and Sitakund Anticline (**c**)

powdered samples were mixed with stearic acid in a 1:10 ratio and pulverized for at least two minutes. The mixture was then ladled into a 30 mm aluminum cap and sandwiched between two tungsten carbide pellets using a manual hydraulic press at 10–15 tons per square inch for 2 min. After slowly releasing the pressure, the pellet was prepared for X-ray analysis. The major elements were determined using an X-ray fluorescence (XRF) spectrometer, following the procedures of Goto and Tatsumi (1994, 1996), with a Rigaku ZSX Primus XRF machine equipped with a 4 kW Rh-anode X-ray tube at the Institute of Mining, Minerals and Metallurgy in Joypurhat, Bangladesh. A voltage of 40 kV and a current of 60 mA were employed to determine the heavy and light elements, respectively. Geological Survey of Japan (GSJ) Stream Sediments and USGS Rock Standards have been used to obtain the results for this study. Analytical uncertainty for major elements is about 2%. About 100 g of each sample was heated at 1000 °C to obtain the loss on ignition (LOI) before the treatment. Table 3 shows the percentage of the major elements for the Tipam sandstones.

4 Results

4.1 Sandstone petrography

The Tipam sandstones are fine- to medium-grained, yellowish-grey to yellowish-brown in color (Fig. 2a–d). Quartz (Q) is the most dominant constituent (59.94%) in the Tipam sandstones and occurs as both monocrystalline and polycrystalline grains. Monocrystalline quartz (Qm) grains (Fig. 3a, b) make up ~ 56.92% of these sandstones. In contrast, polycrystalline quartz (Qp) covers 4.02% of the total lithic grains. Feldspar (F) covers about 8.93% of the total grains, whereas potassium feldspar (6.15%) dominates over the plagioclase feldspar (2.78%).

Table 2 Modal compositions (%) of the Tipam sandstones in the CTFB of the Bengal Basin

Structure	Sample no.	Q		Chert	F		Mica		Ch	L		
		Q_m	Q_p		K	P	WM	B		Ls	Lm	Lv
Bandarban	BB02	42.55	5.29	1.68	13.46	0.72	9.13	6.49	0.72	10.82	2.88	0.00
	BB06	58.41	7.27	3.86	4.32	1.36	6.82	3.41	0.45	9.09	1.36	0.00
	BB09	46.36	7.28	3.40	11.41	3.88	7.52	3.64	0.97	4.13	5.34	0.00
	BB10	51.67	6.22	3.35	3.59	2.87	9.57	8.61	1.44	7.89	2.39	0.00
	BB11	45.43	3.88	6.16	10.96	4.11	9.13	3.88	1.37	7.08	3.42	0.00
	BB12	56.51	6.05	3.02	2.79	4.88	7.67	6.74	0.70	7.91	1.16	0.00
Sitakund	SK01	56.82	6.71	3.36	5.15	1.12	7.16	9.84	0.00	5.15	3.36	0.00
	SK02	49.47	2.96	2.96	8.03	4.23	8.88	8.25	0.42	6.98	5.29	0.00
	SK03	55.01	3.91	4.16	6.36	1.96	8.07	10.76	0.00	5.38	2.20	0.00
	SK04	60.12	3.97	3.97	3.37	3.37	6.75	7.14	0.00	6.55	1.19	0.00
	SK05	61.74	1.69	6.05	2.91	3.15	7.02	7.75	0.00	5.81	1.21	0.00
	SK06	56.89	3.40	4.29	3.76	4.65	7.33	8.59	0.00	5.55	3.94	0.00
	SK07	57.65	4.94	4.94	3.76	2.82	7.06	4.00	0.24	8.00	0.94	0.00
Inani	IN01	58.73	1.42	3.77	8.25	3.07	4.25	4.95	1.18	9.43	3.07	0.00
	IN02	63.43	1.81	4.74	6.32	1.81	2.26	5.19	1.13	7.90	3.16	0.00
	IN03	61.19	1.83	3.42	8.22	2.28	4.79	5.02	0.00	4.57	6.16	0.00
Sitapahar	SP01	65.38	2.42	0.97	2.18	1.45	3.63	8.96	0.73	9.20	1.21	0.00
	SP02	53.88	3.40	0.97	3.64	1.94	6.07	9.22	1.46	10.44	0.73	0.00
	SP04	60.19	4.17	3.01	8.10	2.31	5.09	2.55	0.69	7.87	1.16	0.00
	SP05	57.05	1.74	4.77	6.51	3.69	5.42	7.59	0.65	8.68	0.00	0.00
Maximum		65.38	7.28	6.16	13.46	4.88	9.57	10.76	1.46	10.82	6.16	0.00
Minimum		42.55	1.42	0.97	2.18	0.72	2.26	2.55	0.24	4.13	0.73	0.00
Average		55.92	4.02	3.64	6.15	2.78	6.68	6.63	0.61	7.42	2.51	0.00

Structure	Sample no.	C	Others	Recalculated to 100%			Lt	F+Lt	Qm/Qp	K/P
				Q	F	L				
Bandarban	BB02	1.44	4.81	63.98	18.32	17.70	15.38	29.56	8.04	18.69
	BB06	0.00	3.64	81.17	6.63	12.20	14.31	19.99	8.03	3.18
	BB09	0.24	5.83	69.73	18.69	11.58	12.87	28.16	6.37	2.94
	BB10	0.24	2.15	78.53	8.28	13.18	13.63	20.09	8.31	1.25
	BB11	0.68	3.88	68.45	18.60	12.96	16.66	31.73	11.71	2.67
	BB12	0.70	1.86	79.66	9.32	11.02	12.09	19.76	9.34	0.57
Sitakund	SK01	0.00	1.34	81.90	7.68	10.42	11.87	18.14	8.47	4.60
	SK02	0.42	2.11	69.31	15.34	15.35	15.23	27.49	16.71	1.90
	SK03	0.49	1.71	79.87	10.53	9.60	11.74	20.06	14.07	3.24
	SK04	0.40	3.17	82.46	8.17	9.38	11.71	18.45	15.14	1.00
	SK05	0.48	2.18	84.16	7.20	8.50	13.07	19.13	36.53	0.92
	SK06	0.00	1.61	78.30	10.74	11.51	13.78	22.19	16.73	0.81
	SK07	1.41	4.24	81.31	8.09	10.76	13.88	20.46	11.67	1.33
Inani	IN01	0.00	1.89	72.85	15.54	14.25	16.27	27.59	41.36	2.69
	IN02	0.00	2.26	78.48	10.36	12.40	15.80	23.93	35.04	3.49
	IN03	0.00	2.51	75.78	13.86	12.24	14.15	24.65	33.44	3.61
Sitapahar	SP01	0.00	3.87	83.05	4.37	12.57	11.38	15.01	27.02	1.50
	SP02	0.00	8.25	77.67	7.18	14.89	12.14	17.72	15.85	1.88
	SP04	0.00	4.86	77.61	13.41	10.40	12.04	22.45	14.43	3.51
	SP05	0.43	3.47	77.10	13.23	10.53	13.45	23.65	32.79	1.76
Maximum		1.44	8.25	84.16	18.60	17.70	16.66	31.73	41.36	18.69
Minimum		0.00	1.34	63.98	4.37	8.50	11.71	15.01	6.37	0.57
Average		0.35	3.28	77.00	11.00	12.00	13.57	22.51	18.55	3.08

Qm-monocrystalline quartz, Qp-Poly crystalline quartz, K-k-feldspar, P-plagioclase, WM-white mica, B-biotite, Ls-sedimentary lithic grains, Lm-metamorphic lithic grain, Lv-volcanic lithic grain, Ch-chlorite, Lt-total lithic grains + Qp, Lvm-lithic meta-volcanic, Lsm-lithic meta-sedimentary

Table 3 Geochemical compositions (%) of the Tipam sandstones from the CTFB of the Bengal Basin

Sample no.	BB01	BB02	BB03	BB06	BB07	BB09	BB10	BB11	BB12	SK01	SK02	SK03
SiO2	81.59	82.38	84.43	79.64	75.65	70.32	75.66	74.97	74.76	71.81	70.75	73.91
TiO2	0.54	0.62	0.54	0.51	0.67	0.69	0.47	0.73	0.74	0.84	0.79	0.66
Al2O3	7.73	8.42	6.67	9.50	10.54	13.19	10.24	11.03	10.22	13.44	13.68	14.39
Fe2O3	7.74	3.30	6.36	5.46	6.72	9.88	7.31	7.00	8.19	8.51	7.76	6.06
MnO	0.18	0.15	0.00	0.10	0.12	0.14	0.18	0.12	0.16	0.14	0.13	0.06
MgO	0.11	0.15	0.00	0.22	0.59	0.71	0.62	0.68	0.52	0.58	0.78	0.25
CaO	0.13	0.15	0.07	0.94	1.70	1.15	1.40	1.20	1.53	0.83	1.49	0.50
Na2O	0.11	0.24	0.16	0.62	0.78	0.79	1.12	1.17	0.82	0.65	1.03	0.36
K2O	1.82	2.11	1.73	2.98	3.16	3.04	2.92	2.99	2.95	3.12	3.47	3.75
P2O5	0.06	0.08	0.05	0.02	0.08	0.10	0.08	0.12	0.11	0.08	0.11	0.07
F1	−1.73	−5.16	−3.17	−3.17	−2.09	1.53	−1.22	−1.72	−1.01	0.21	−0.26	−1.40
F2	−5.32	−3.57	−5.01	−2.01	−1.78	−2.91	−2.03	−1.78	−2.36	−2.56	−1.26	−1.27
K2O/Na2O	16.33	8.95	11.09	4.85	4.07	3.84	2.60	2.57	3.58	4.82	3.36	10.55
Fe2O3 + MgO	7.85	4.17	6.36	5.68	7.30	10.58	7.93	7.68	8.71	9.09	8.54	6.31
Al2O3/SiO2	0.09	0.10	0.08	0.12	0.14	0.19	0.14	0.15	0.14	0.19	0.19	0.19
Al2O3/(CaO + Na2O)	32.51	21.60	29.59	6.11	4.26	6.79	4.05	4.66	4.33	9.08	5.41	16.92
SiO2/Al2O3	10.56	9.78	12.65	8.38	7.18	5.33	7.39	6.80	7.32	5.34	5.17	5.14
Fe2O3 + MgO	7.73	4.09	6.32	5.64	7.27	10.47	7.86	7.60	8.63	9.00	8.47	6.26
Al2O3/TiO2	14.38	13.51	12.28	18.50	15.67	19.12	21.87	15.15	13.85	16.04	17.38	21.64
Log (Na2O/K2O)	−1.21	−0.95	−1.04	−0.69	−0.61	−0.58	−0.41	−0.41	−0.55	−0.68	−0.53	−1.02
Log (SiO2/Al2O3)	1.02	0.99	1.10	0.92	0.86	0.73	0.87	0.83	0.86	0.73	0.71	0.71
Log (Fe2O3/K2O)	0.63	0.43	0.57	0.26	0.33	0.51	0.40	0.37	0.44	0.44	0.35	0.21
CIA	77.42	75.35	75.65	61.69	58.09	67.16	59.87	60.96	63.36	69.93	63.38	72.79
PIA	95.37	92.81	94.59	70.15	62.99	75.79	62.66	67.08	64.34	80.75	70.52	88.65
CIW	96.51	94.65	96.05	78.08	71.59	80.66	70.83	74.27	72.42	84.86	76.73	91.58
ICV	1.37	1.08	1.33	1.15	1.35	1.29	1.41	1.31	1.50	1.12	1.18	0.82

Sample no.	SK04	SK06	SK07	IN01	IN02	IN03	SP01	SP02	SP04	SP05	Avg
SiO2	72.99	69.11	68.48	77.57	77.49	77.73	71.54	71.53	73.14	74.34	74.99
TiO2	0.87	0.99	1.28	0.75	0.62	0.58	0.63	0.96	0.97	0.84	0.74
Al2O3	11.85	13.54	13.53	9.87	9.85	9.74	14.32	11.62	12.00	11.83	11.24
Fe2O3	7.41	8.80	10.02	6.16	7.05	7.48	7.77	9.42	10.22	7.44	7.55
MnO	0.07	0.11	0.00	0.00	0.00	0.14	0.12	0.17	0.23	0.11	0.11
MgO	1.28	1.42	1.19	0.46	0.54	0.44	0.38	0.60	0.29	0.45	0.56
CaO	0.97	1.04	1.08	1.11	0.72	0.57	0.81	1.40	0.45	0.92	0.92
Na2O	1.26	1.18	0.84	0.83	0.66	0.55	0.92	0.71	0.00	0.72	0.70
K2O	3.18	3.55	3.43	3.25	2.99	2.71	3.44	3.47	2.63	3.34	3.00
P2O5	0.13	0.27	0.16	0.00	0.07	0.06	0.07	0.11	0.07	0.00	0.08
F1	−2.38	−1.16	−0.41	−3.32	−2.56	−1.87	0.57	−0.52	0.87	−1.57	−1.43
F2	−2.14	−2.04	−2.61	−1.56	−2.72	−3.37	−1.35	−2.04	−4.53	−1.80	−2.55
K2O/Na2O	2.53	3.00	4.09	3.92	4.55	4.93	3.75	4.87	–	4.64	5.37
Fe2O3 + MgO	8.69	10.22	11.21	6.62	7.59	7.92	8.15	10.02	10.51	7.89	8.14
Al2O3/SiO2	0.16	0.20	0.20	0.13	0.13	0.13	0.20	0.16	0.16	0.16	0.15
Al2O3/(CaO + Na2O)	5.32	6.10	7.05	5.08	7.13	8.72	8.31	5.51	26.47	7.22	10.56
SiO2/Al2O3	6.16	5.11	5.06	7.86	7.87	7.98	4.99	6.15	6.10	6.28	7.03
Fe2O3 + MgO	8.62	10.15	11.13	6.57	7.51	7.86	8.05	9.90	10.37	7.80	8.06
Al2O3/TiO2	13.60	13.68	10.61	13.13	15.82	16.83	22.79	12.07	12.41	14.04	15.65
Log (Na2O/K2O)	−0.40	−0.48	−0.61	−0.59	−0.66	−0.69	−0.57	−0.69	–	−0.67	−0.67
Log (SiO2/Al2O3)	0.79	0.71	0.70	0.90	0.90	0.90	0.70	0.79	0.79	0.80	0.83
Log (Fe2O3/K2O)	0.37	0.39	0.47	0.28	0.37	0.44	0.35	0.43	0.59	0.35	0.41

Table 3 (continued)

Sample no.	SK04	SK06	SK07	IN01	IN02	IN03	SP01	SP02	SP04	SP05	Avg
CIA	63.03	65.82	66.97	58.83	64.26	67.31	68.71	61.68	77.37	64.64	66.56
PIA	70.55	75.24	76.82	65.22	74.69	79.12	79.11	69.44	93.24	74.21	76.52
CIW	77.15	80.92	82.03	74.46	81.47	84.44	83.65	77.06	94.76	80.56	82.03
ICV	1.37	1.36	1.41	1.32	1.33	1.31	1.00	1.48	1.24	1.20	1.27

After quartz, micas (13.31%) are the dominant constituents in the Tipam sandstones, where white mica (WM, Fig. 3a, c, f) and biotite (B, Fig. 3b) occur in almost equal amounts with 6.68% and 6.63%, respectively. Among the lithic grains (L), sedimentary grains (L_s) dominate in the investigated sandstones with an average value of 7.42%. Ls grains (Fig. 3d) are present as shale, siltstone, and chert. Metamorphic rock fragments (L_m) comprise 2.51% of the detrital grains, and commonly occur as mica-schist (Fig. 3b), graphite-schist, quartz-mica schist, quartz-graphite-schist, quartz-graphite-mica schist (Fig. 3e), etc. However, volcanic lithic grains were not identifiable in the investigated sandstones. Chert (Fig. 3f) constitutes 3.64% of the total framework grains.

Chlorite grains (Ch) occur in minor amounts (0.61%). Detrital carbonate (C) is present only in a few samples (avg. 0.35%). The sandstones contain a small amount of matrix. Clays (Fig. 3d) are the dominant cement in the studied sandstones.

4.2 Major element geochemistry

The geochemical analysis reveals the highest concentrations of SiO_2 with an average value of 74.99% (Table 3). Next to SiO_2, Al_2O_3 is the dominant oxide in the Tipam sandstones, where the values range from 6.67 to 14.39% (avg. 11.24%). The concentration of Fe_2O_3 is relatively high (average 7.58%) and attains a wide range from 5.42 to 10.08%. The concentration of K_2O (avg. 3.00%) dominates over the Na_2O (0.70%). The average content of CaO and MgO represents 0.92% and 0.56%, respectively. The higher concentration of K_2O and lower values of Na_2O and CaO are congenial with the higher percentage of K-feldspar than plagioclase feldspar. TiO_2 presents as a minor amount with an average value of 0.74%. The concentrations of MnO (avg. 0.11%) and P_2O_5 (avg. 0.08%) are very low in the Tipam sandstones.

The linear correlation matrix of the major oxides against Al_2O_3 for the Tipam sandstones is displayed in Table 4, where almost all the elements show positive correlations except SiO_2. The strong negative correlation of SiO_2 ($r = -0.92$) with Al_2O_3 suggests that hydrodynamic fractionation and sorting effects may control their distribution (Hossain, 2019). On the other hand, the moderate positive correlation between Al_2O_3 and Fe_2O_3 ($r = 0.49$) suggests an increase in aluminous clays or heavy minerals in the weathering products (Hossain et al., 2017). The strong positive correlations of Al_2O_3 with TiO_2 ($r = 0.69$), and P_2O_5 ($r = 0.50$) suggest the presence of heavy minerals in the investigated sandstones (Sayem et al., 2023). The positive correlations of MgO ($r = 0.55$), CaO ($r = 0.38$), Na_2O ($r = 0.45$), and K_2O ($r = 0.83$) indicate that these oxides are associated with phyllosilicate minerals (Hossain, 2019). MnO exhibits a very poor relationship ($r = 0.09$) with Al_2O_3.

The major element concentrations of the Tipam sandstones were normalized to the upper continental crust (UCC, Taylor & McLennan, 1985) values and displayed in Fig. 4. In general, most of the major oxides are depleted relative to the upper continental crust values. The SiO_2 concentration is slightly higher than the UCC value, indicating higher concentrations of quartz-rich sediments. In contrast, Al_2O_3 is slightly depleted, probably with lesser amounts of clay components in the studied sandstones (Hossain, 2019; Sayem et al., 2023). Most of the sandstones are enriched in TiO_2, Fe_2O_3, and MnO probably due to the presence of a higher proportion of aluminosilicate minerals and iron cement (Sayem et al., 2023). The strong depletion of MgO, CaO, and Na_2O represents lesser concentrations of plagioclase feldspar in the investigated samples, which agreed well with the petrographic results (Table 2).

5 Discussions

5.1 Sediment classification and maturity

The sandstone classification proposed by McBride (1963) is widely accepted, where he classified sandstones using the QFL plot. The average detrital composition of the Tipam sandstones is $Q_{77}F_{11}L_{12}$. According to this QFL diagram, the examined sandstones are primarily categorized as sublitharenite, with a few samples appearing in the lithic subarkose field (Fig. 5a). Additionally, the scatter plot of $\log(SiO_2/Al_2O_3)$ versus $\log(Fe_2O_3/K_2)$, commonly employed for sandstone classification (Herron, 1988), which indicate that the Tipam sandstones are predominantly litharenite. However, a few samples are scattered in the Fe-sand field (Fig. 5b). The petrographic and geochemical data are also used to determine sediment maturity. Long et al. (2012)

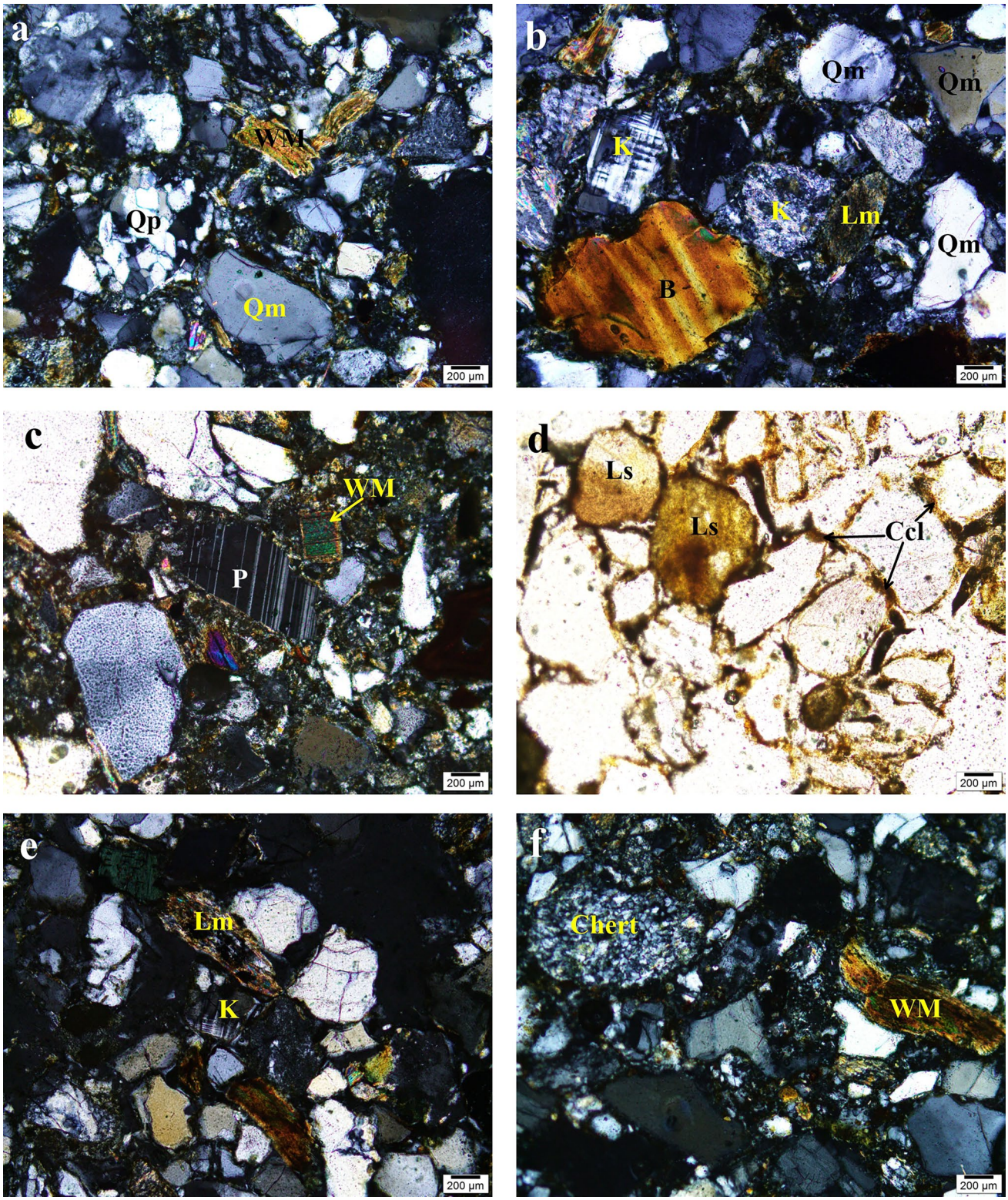

Fig. 3 Photomicrographs showing the detrital composition of the Tipam sandstones: **a** monocrystalline quartz (Qm), polycrystalline quartz (Qp), and white mica (WM); **b** K-feldspar (K), biotite (B), mica-schist (Lm); **c** angurlar to subangular plagioclase feldspar (P), and white mica (WM); **d** sedimentary lithic grains (Ls), and clay cement (Ccl); **e** graphite-mica schist (Lm), and K-feldspar; **f** chert and white mica (WM)

Table 4 Linear correlation matrix of the major oxides of the Tipam sandstones from the CTFB of the Bengal Basin

	SiO_2	Al_2O_3	Fe_2O_3	CaO	MgO	Na_2O	K_2O	MnO	TiO_2	P_2O_5
SiO_2	1.00									
Al_2O_3	−0.92	1.00								
Fe_2O_3	−0.70	0.49	1.00							
CaO	−0.58	0.38	0.22	1.00						
MgO	−0.74	0.55	0.46	0.55	1.00					
Na_2O	−0.58	0.45	0.08	0.76	0.78	1.00				
K_2O	−0.81	0.83	0.21	0.65	0.58	0.65	1.00			
MnO	−0.13	0.09	0.37	−0.05	−0.16	−0.16	−0.16	1.00		
TiO_2	−0.85	0.69	0.68	0.50	0.69	0.42	0.70	0.03	1.00	
P_2O_5	−0.64	0.50	0.51	0.32	0.82	0.50	0.38	0.11	0.50	1.00

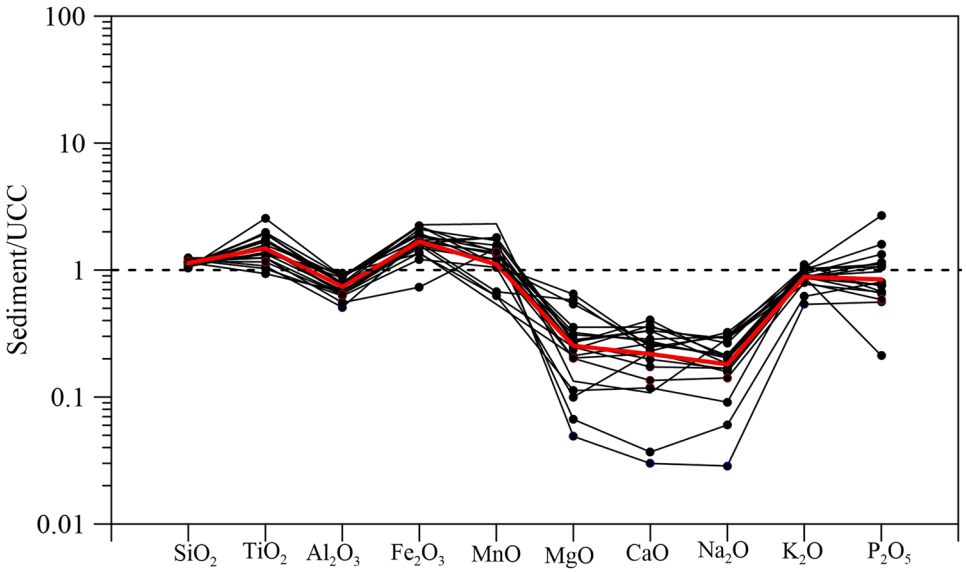

Fig. 4 Major element concentrations of the Tipam sandstones normalized to Upper Continental Crust (UCC) values (*after* Taylor & McLennan, 1985). The red line indicates the average depletion/enrichment of the major oxides

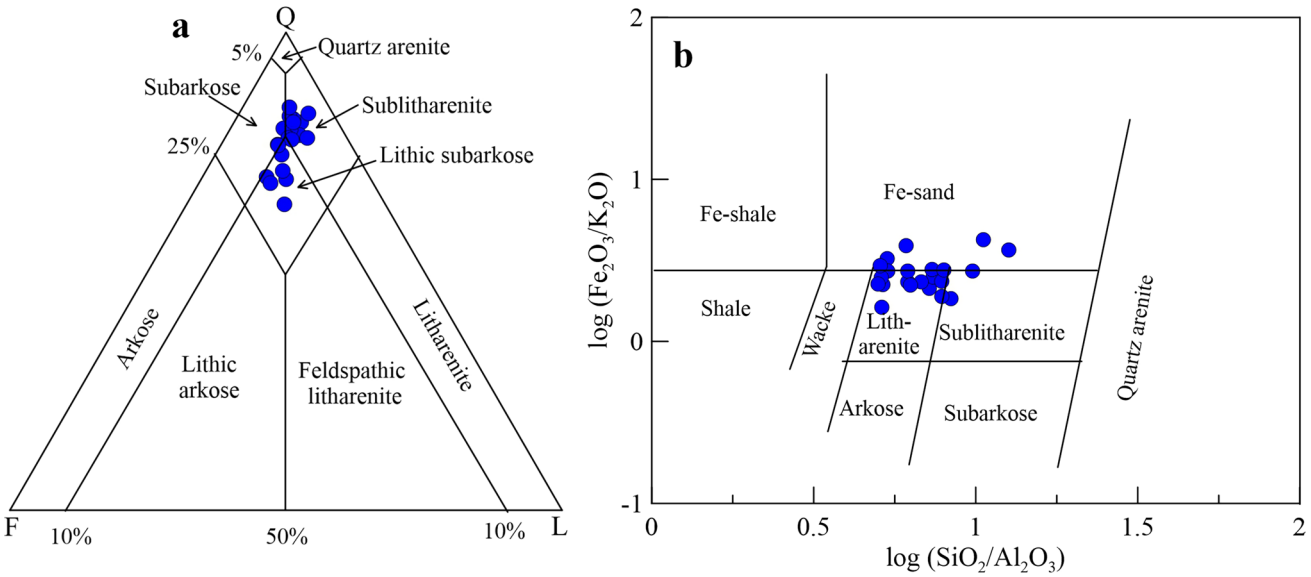

Fig. 5 Classification of the Tipam sandstones: **a** detrital classification *after* McBride (1963); **b** geochemical classification *after* Herron (1988)

introduced the ICV (index of compositional variability) to measure sediment maturity, where the ICV > 1.0 indicates immature sediments, and vice versa. The ICV value for the investigated sandstones ranges between 0.82 and 1.50, with an average of 1.27 (Table 3), indicating immature sandstone. The bivariate plot of ICV vs. CIA (Long et al., 2012) also reflects that the Pliocene Tipam sandstones are predominantly immature (Fig. 6a).

Potter (1978) correlated the $SiO_2/A1_2O_3$ ratio with total quartz (Qt), and total feldspar plus total rock fragments (F + Lt) to examine the sediment maturity. SiO_2/Al_2O_3 is used to assess the relative abundance of silica (SiO_2) to alumina (Al_2O_3) in sandstones. The ratio is very high for quartz arenites and low for immature sandstones (Potter, 1998). Quartz is very resistant to weathering and often dominates in well-rounded and well-sorted mature sandstones. In contrast,

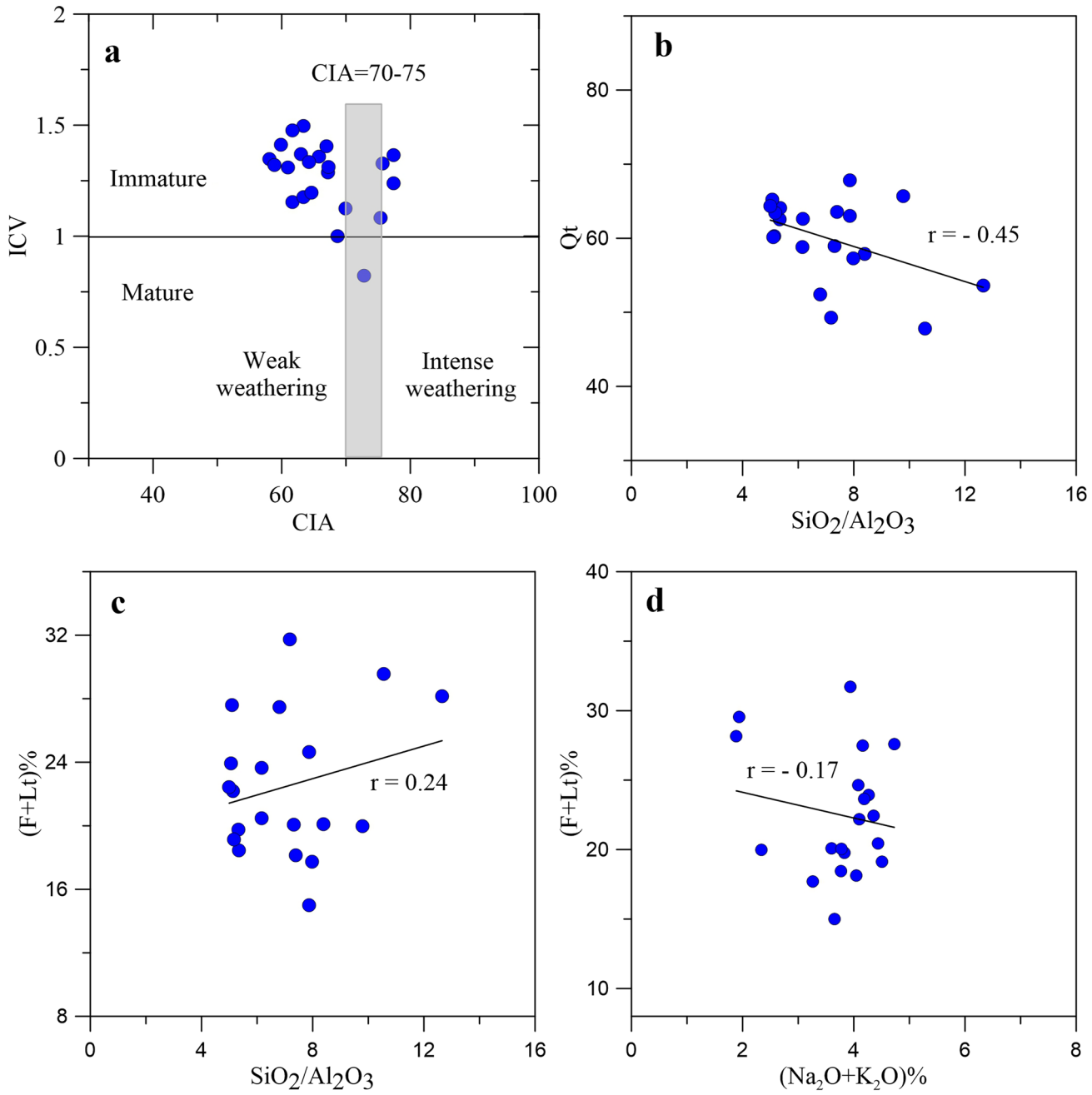

Fig. 6 Sandstone maturity diagrams of **a** CIA (Chemical Index of Alteration) versus ICV (Index of Compositional Variability) (*after* Long et al., 2012); **b** Si_2O/Al_2O_3 versus Qt (*after* Potter, 1978); **c** Si_2O/Al_2O_3 versus (F + Lt) (*after* Potter, 1978); **d** ($Na_2O + K_2O$) versus (F + Lt) (*after* Pettijohn et al., 1972)

feldspar (F) and lithic grains (Lt) are less resistant to weathering and are usually incorporated in immature sandstones. Thus, for mature sandstone, total quartz content (Qt) shows a positive correlation with SiO_2/Al_2O_3. On the other hand, a negative correlation exists between (F + Lt) and SiO_2/Al_2O_3. The results of this study show a moderate negative correlation (r = − 0.45) between SiO_2/Al_2O_3 and Qt (Fig. 6b), whereas a moderate positive correlation (r = 0.24) persisted between SiO_2/Al_2O_3 and F + Lt (Fig. 6c). These results indicate that the investigated sandstones are compositionally immature. In addition, the alkali content ($Na_2O + K_2O$) is very much applicable for the index of chemical maturity (Pettijohn, et al., 1972), where ($Na_2O + K_2O$) is positively correlated with (F + Lt) for mature sandstones. This relationship shows a negative correlation (r = − 0.17) for the investigated sandstones, which further supports the immature nature. Furthermore, angular to subangular grains (Fig. 3) and a relatively higher abundance of unstable feldspar and ductile grains indicate an immature nature. The immature nature of the investigated sandstones suggests that they were deposited close to their source region (Boggs, 2009).

5.2 Provenance

Prior to the collision, the Bengal Basin sourced its sediments from the Indian Craton in the Early Cenozoic (Uddin & Lundberg, 1998). The collision between the Indian and Eurasian plates resulted in the uplift of the Himalayas during the Oligocene–Miocene period (Critelli & Garzanti, 1994; Garzanti et al., 1987; Najman et al., 2012; Searle et al., 1999; Yang et al., 2019). Many of the Himalayan rivers, including the paleo-Brahmaputra, originated from the southern slopes of the Himalayas. These rivers transported detritus from the Higher and Lesser Himalayas, depositing it in the Sub-Himalayan Neogene foreland basins (Bracciali et al., 2015; Garzanti & Andò, 2007). During the Miocene, the paleo-Brahmaputra River mainly carried Himalayan and Trans-Himalayan sediments into the Bengal Basin (Bracciali et al., 2015; Garzanti & Andò, 2007; Najman et al., 2012; Rahman et al., 2020; Uddin & Lundberg, 1998; Yang et al., 2019). The river changed its course due to the uplift of the Shillong Plateau in the Pliocene–Pleistocene (Johnson & Alam, 1991), which led to the southward advance of the Eastern Himalaya's deformation front. Meanwhile, the deformation front of the Indo-Burman Ranges (IBR) progressively moved westward and began contributing IBR detritus to the Bengal Basin (Rahman et al., 2020; Uddin & Lundberg, 1998; Yang et al., 2019) during the Pliocene–Pleistocene period.

The modal composition of clastic rocks serves as a valuable clue in understanding their provenance (Dickinson & Suczek, 1979; Ingersoll & Suczek, 1979; Dickinson, 1985). The triangular diagrams of QFL and Q_mFL_t are commonly used to distinguish recycled orogen, continental block, and magmatic arc provenances (Dickinson, 1985). According to the QFL diagram, the analyzed samples suggest a recycled orogen source (Fig. 7a). Meanwhile, the $QmFL_t$ diagram reveals a predominance of high monocrystalline quartz and feldspar, and a moderate level of lithic grains, characteristics of quartzose recycled provenance (Fig. 7b).

Apart from modal composition, the provenance of clastic rocks also mirrored their geochemical composition (Armstrong-Altrin et al., 2021; Hayashi et al., 1997; Li et al., 2020; Nesbitt & Young, 1982, 1984; Rahman et al., 2020; Roser & Korsch, 1986, 1988; Sayem et al., 2023; Suttner & Dutta, 1986; Yeasmin et al., 2024). Based on major element composition, Roser and Korsch (1988) proposed a provenance discriminant function diagram which is divided into four distinct provenance types, such as felsic igneous, intermediate igneous, mafic igneous, and quartzose recycled. Within this diagram, the majority of the studied samples are dispersed prominently within the quartzose recycled field (Fig. 7c), with two samples plotted within the mafic igneous source, and two in the intermediate igneous. Although only one sample scatter at the felsic field most of the samples show affinity along the boundary between the quartzose sedimentary and felsic igneous provenances.

The Al_2O_3/TiO_2 is graphed against SiO_2 (Le Bas et al., 1986) to delineate the source rock composition. This diagram (Fig. 7d) displays that felsic igneous is the dominant source for the Tipam Sandstone Formation. In addition, the TiO_2/Zr ratio (Hayashi et al., 1997) serves as another valuable proxy in determining the provenance of clastic rocks, with values below 55 indicative felsic igneous, between 55 and199 suggesting intermediate igneous, and values exceeding 200 pointing to mafic igneous sources. For the Tipam sandstones, the TiO_2/Zr ratio ranges between 5.91 and 39.67 (Table 3), indicating a felsic igneous provenance. Conversely, the metamorphic lithic grains (Lm) in the studied sandstones indicate the presence of meta-sedimentary and metamorphic source rocks.

Based on the above discussions, it is evident that the Tipam sandstones were derived predominantly from recycled sedimentary/meta-sedimentary, felsic igneous, and metamorphic sources. The abundance of K-feldspar (Table 2) in the Pliocene Tipam sandstones, compared to Miocene Surma Group sandstones (Dina et al., 2016; Sayem & Rahman, 2012), suggests a granitic source, likely derived from deep crustal Higher Himalayan Crystalline Sequence (HHCS, Uddin & Lundberg, 1998). The absence of granitic terrain in the IBR devoids the possibility of it being a source rock for the Pliocene sediments in the Bengal Basin. Additionally, the absence of volcanic lithic fragments (Lv) excludes the IBR as a potential source. In contrast, angular to subangular shape, and fresh feldspars (Fig. 3b, c) suggest nearby sources, indicating that the

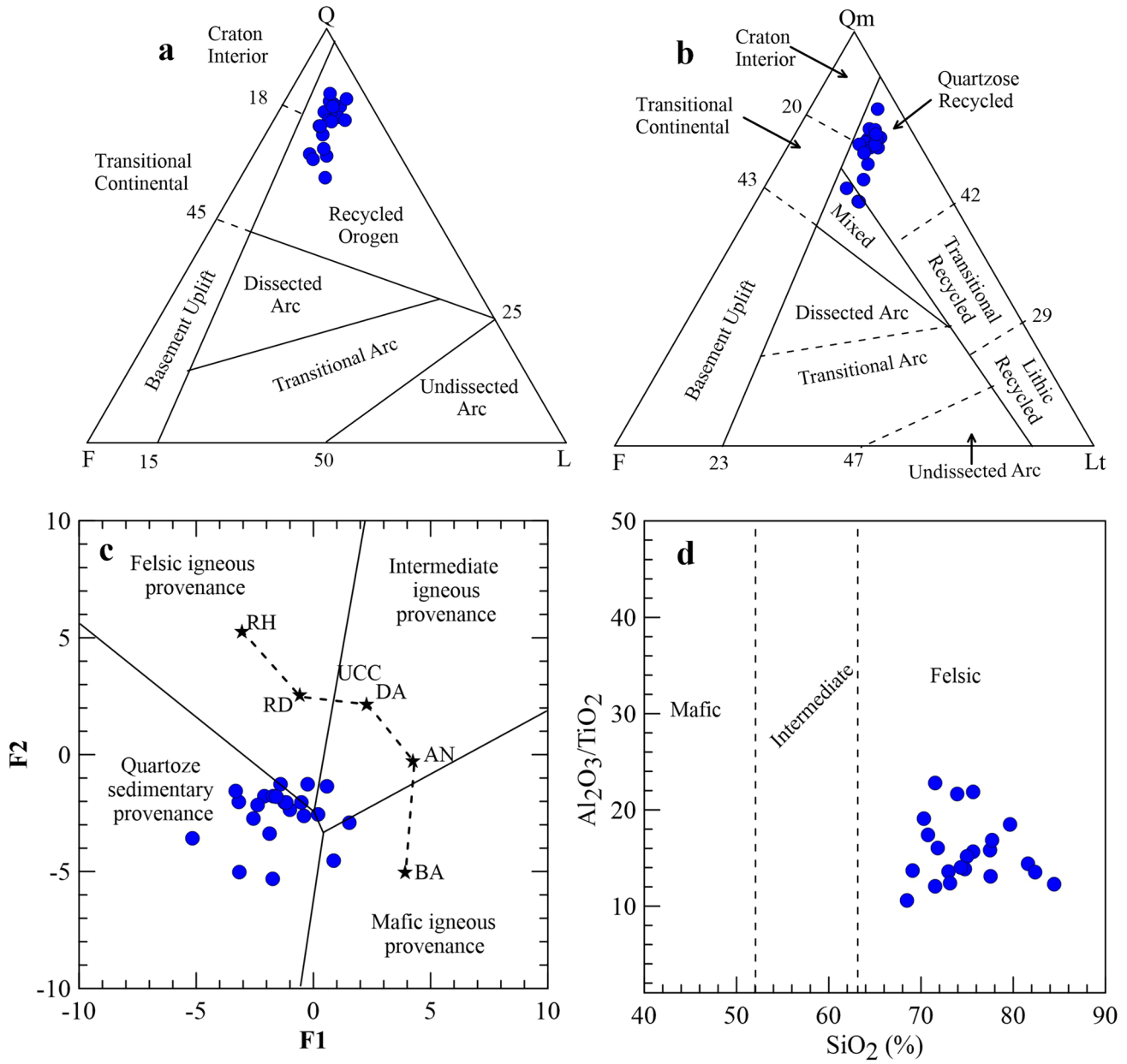

Fig. 7 Provenance discriminating diagrams for the Tipam sandstones: **a**, **b** Q–F–L and Q_m–F–L_t triangular plots (*after* Dickinson, 1985); **c** major element discrimination function F1 versus F2 (*after* Roser & Korsch, 1988); **d** bivariate diagram of SiO_2 versus Al_2O_3/TiO_2 (*after* Le Bas et al., 1986)

Sub-Himalayan sedimentary and the IBR may be potential sources of the Tipam sandstones. Rahman et al. (2020) identified younger zircon ages (< 200 ma) in the Tipam sandstones from the CTFB, suggesting IBR as a possible source. The rich of monocrystalline quartz, sedimentary and metamorphic lithic fragments (Table 2), points to the Lesser Himalayan Sequence (LHS) as a potential source, which is composed of sedimentary and low-grade metamorphic rocks (Singh, 2010; Uddin & Lundberg, 1998). Geochemical relationships among various major oxides can also reveal the dominant source area (Singh, 2010). The scatter plot of Na_2O vs. K_2O (Fig. 8a) highlights LHS as a dominant source. The CaO versus TiO_2 plot also indicates a significant contribution of sediments from the LHS (Fig. 8b), with only two samples representing HHCS. Therefore, the mineralogical and geochemical findings of this study indicate that the CTFB primarily sourced its sediments from the LHS, with smaller contributions from the HHCS, Sub-Himalayan sources, and the IBR during the Pliocene.

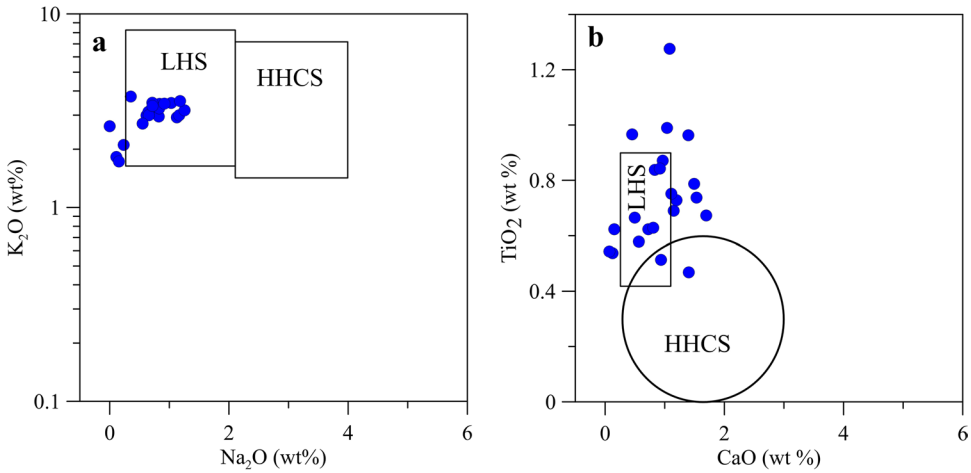

Fig. 8 Source area discrimination diagrams (**a**, **b**) for the Tipam Sandstone Formation (fields are *after* Singh, 2010), where LHS, Lesser Himalayan Sequence; HHCS, Higher Himalayan Crystalline Sequence

5.3 Paleoweathering

Different chemical indices were employed to assess the degree of chemical weathering (Table 3). Chemical Index of Alteration (CIA) reflects the progressive transformation of feldspar into clay minerals (Nesbitt & Young, 1982). CIA values for the sandstones of the Tipam Formation range from 58.09 to 77.42, averaging 66.56, suggesting that these sandstones likely originated from a weak to moderately weathered region. Likewise, the Chemical Index of Weathering (CIW) (Harnois, 1988) assesses the extent of feldspar alteration into clay minerals. CIW values span from 70.83 to 96.51, with an average value of 82.03, indicating moderate chemical weathering. On the other hand, Fedo et al. (1995) suggested the Plagioclase Index of Alteration (PIA) as an alternative to CIW, which aims to specifically clarify plagioclase weathering. PIA values for the studied sandstones ranging between 62.66 and 95.37 (average 76.52) indicate weak to moderate weathering.

Besides the weathering indices, the A–CN–K and (A–K)–C–N diagrams (Fig. 9a, b), also reflect weak to moderate chemical weathering in the source area for the Tipam sandstones. Similarly, the ICV versus CIA diagram (Fig. 6a) also reveals weak to moderate chemical weathering. The weathering intensity of the investigated sandstone is further assessed by the A–CNK–FM triangular plot (Fig. 9c; Nesbitt & Young, 1982), where the samples fall above the feldspar-chlorite but below feldspar-smectite join line. These results further suggest a weak to moderate weathering profile in the source area. The MFW (mafic–felsic–weathering) triangular plot is used to assess the degree of chemical weathering (Ohta & Arai, 2007), where the "M" and "F" and "W" apexes indicate mafic, felsic, weathering parent igneous rocks, respectively. In this plot (Fig. 9d), the Tipam sandstone samples are scattered at a considerable distance from the granite-basalt join line and show moderate to strong weathering trends toward the proximity of the weathering apex (W). Although most of the weathering indices and discriminant diagrams show weak to moderate chemical weathering for the investigated samples only a few samples suggest strong weathering as reflected in the PIA values as well as in Fig. 9d. These variations in weathering intensity across different samples might be linked with the complex interplay of weathering processes and sediment recycling.

The relative abundances of quartz, feldspar, and lithic grains in sandstones have frequently been used to demonstrate the paleoclimate conditions of the provenance (Basu, 1985; Suttner & Dutta, 1986; Yeasmin et al., 2024). One of the simplest methods for interpreting source-area climate is to use a bivariant plot of Qp(F + Lt) versus Qt(F + Lt) (Suttner & Dutta, 1986). This diagram primarily suggests sub-humid climate conditions in the source areas of the Tipam sandstones (Fig. 10a). On the other hand, the ln(Q/L) ln(Q/F) plot by Weltje et al. (1998) indicates that the sediments of the Tipam Sandstone Formation were eroded from slightly weathered source rocks in areas with moderate relief and sub-humid climate condition (Fig. 10b).

5.4 Tectonic setting

The tectonic environment of a depositional basin is widely inferred by analyzing the modal composition of clastic rocks (Dickinson, 1985; Dickinson & Suczek, 1979; Ingersoll & Suczek, 1979; Yeasmin et al., 2024). $Q_pL_{vm}L_{sm}$ and LmLvLs triangular plots (Ingersoll & Suczek, 1979) are commonly used to differentiate different kinds of tectonic settings. According to the $Q_pL_{vm}L_{sm}$ plot, the Tipam Formation sandstones are indicative of collision orogen (Fig. 11a). A suture belt setting is suggested by comparatively higher Ls, low Lm, and absence of Lv lithic grains (Fig. 11b; Table 2). The collision orogen and suture belt settings is indicative of active continent margin (Dickinson, 1985; Dickinson & Suczek, 1979; Ingersoll & Suczek, 1979).

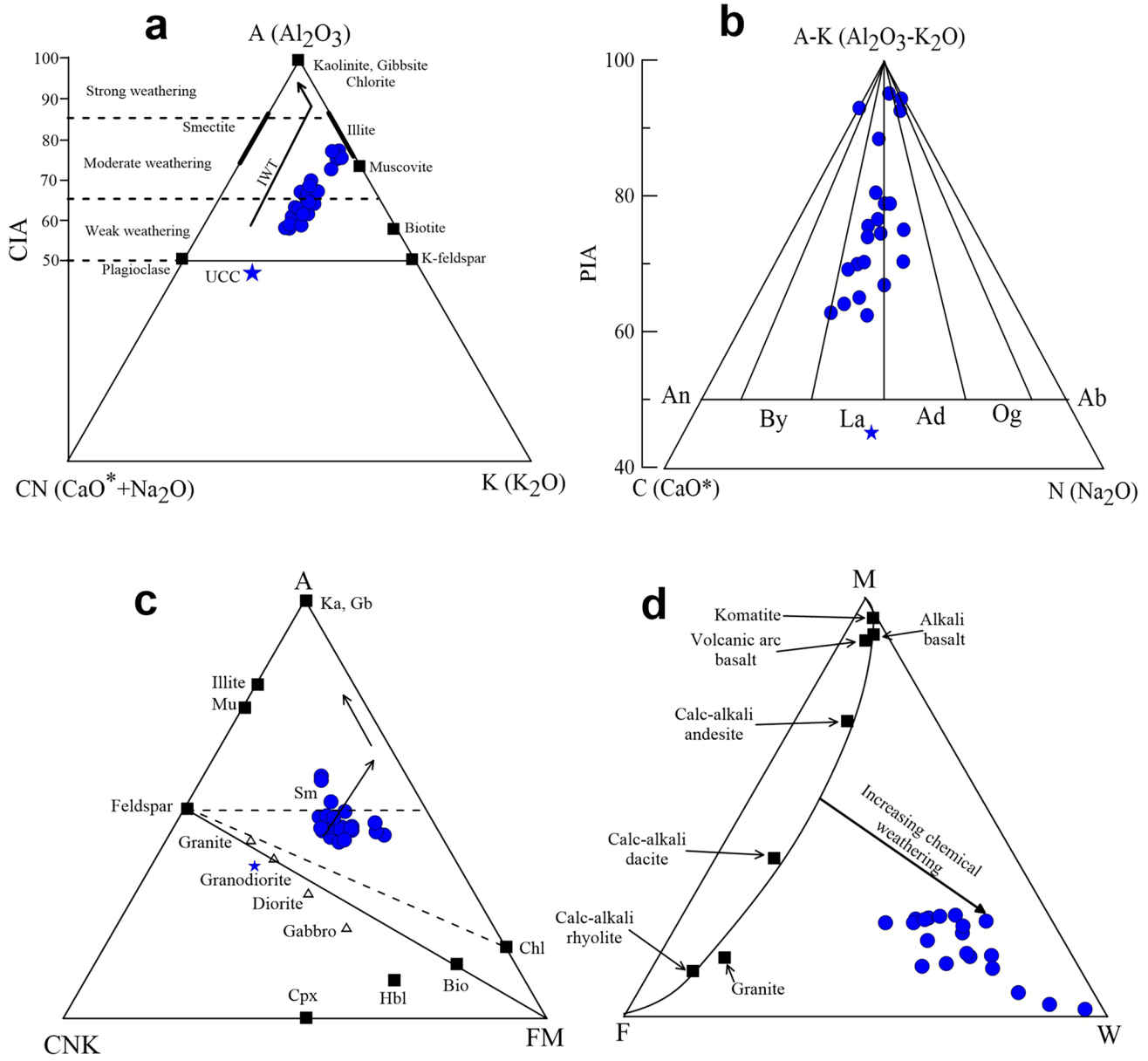

Fig. 9 Triangular plots of: **a** $A(Al_2O_3)-CN(CaO^*+Na_2O)-K(K_2O)$ (Nesbitt & Young, 1984); **b** $(A–K)(Al_2O_3-K_2O)-C(CaO^*)-N(Na_2O)$ (Fedo et al., 1995); **c** $A(Al_2O_3)-CNK(CaO^*+Na_2O+K_2O)-FM(Fe_2O_3+MgO)$ (Ohta & Arai, 2007); where, CaO*, CaO in silicate phase; IWT, ideal weathering trend; UCC, upper continental crust composition; Ka, kaolinite; Gb, gibbsite; Chl, chlorite; Sm, smectite; Mu, muscovite; Pl, plagioclase feldspar; Ksp, K-feldspar; An, anorthite; By, bytownite; La, labradorite; Ad, andesine; Og, oligoclase; Ab, albite; Bio, biotite; Hbl, hornblende; Cpx, clinopyroxene; M, mafic igneous rock; F, felsic igneous rock; W, weathering of parent rocks

The geochemical concentrations are also important for tectonic setting delineation (Bhatia, 1983; Bhatia & Crook, 1986; Murphy, 2000; Roser & Korsch, 1986; Verma & Armstrong-Altrin, 2013). The tectonic discriminate diagram of Roser and Korsch (1986) favors an active margin tectonic setting for Tipam sandstones (Fig. 11c). The active margin setting is also confirmed by SiO_2/Al_2O_3 versus log (K_2O/Na_2O) diagram (Murphy, 2000) (Fig. 11d). Despite a few samples being spread out in a passive margin environment in both diagrams, this aligns with the tectonic past of the Himalayan Orogen. Prior to the collision of the Indian and Eurasian Plates, the northern part of the Indian Plate exhibited a passive margin environment, where Paleozoic to Early Cenozoic sedimentary rocks were laid down along the Tethyan Himalaya (Garzanti et al., 1987; Najman et al., 2012; Uddin & Lundberg, 1998). These rocks began to rise

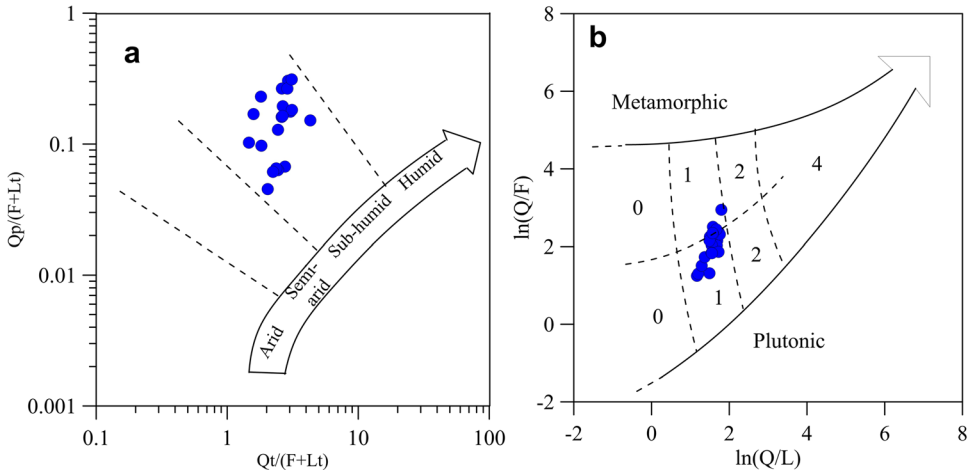

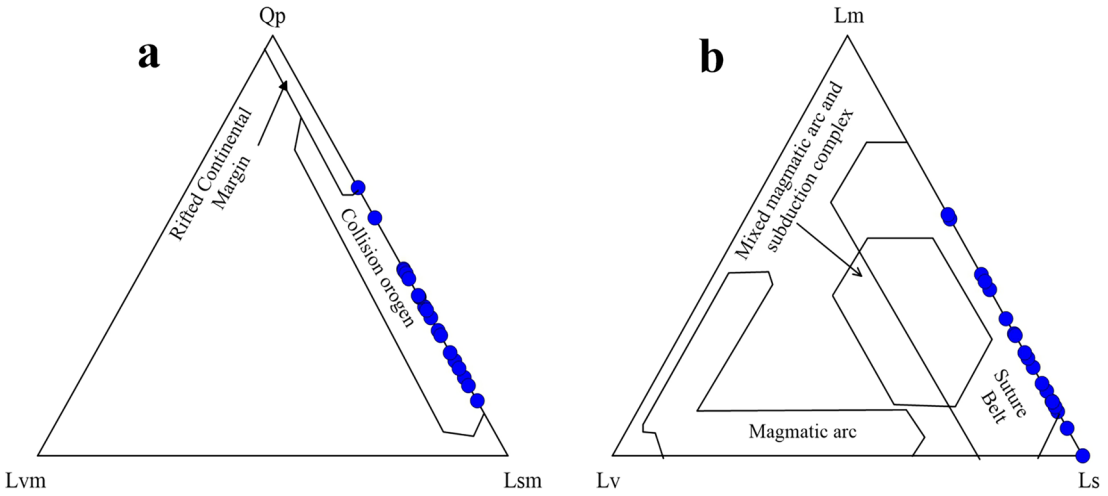

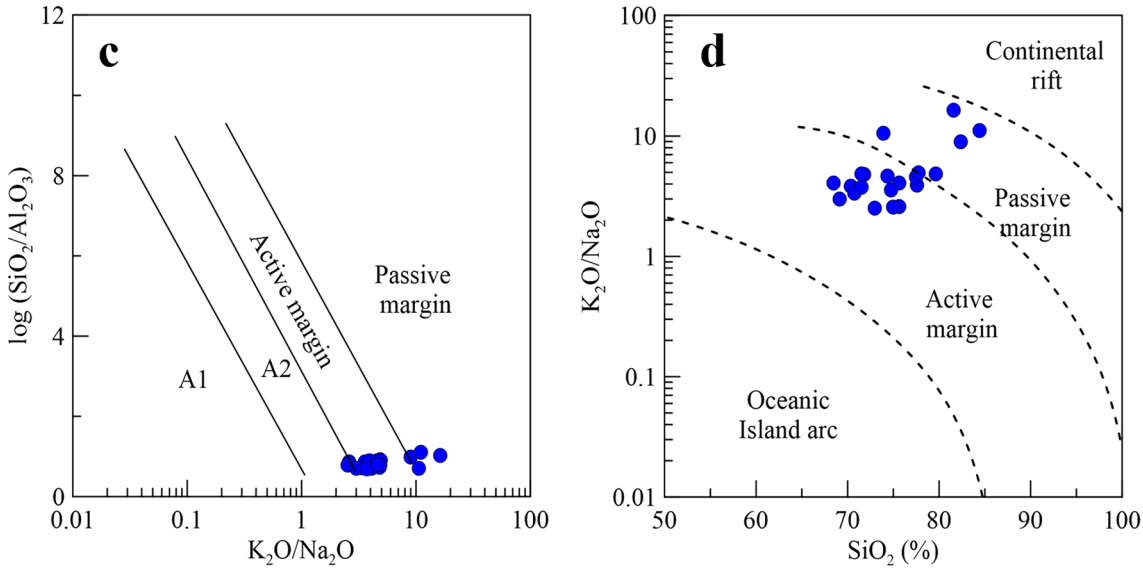

Fig. 10 The scatter plots displaying the paleoclimate conditions: **a** Qt/(F + Lt) versus Qp/(F + Lt) after Suttner and Dutta (1986); **b** ln (Q/L) versus ln (Q/F) after Weltje et al. (1998), where, 0, arid climate, high relief, unweathered; 1, sub-humid climate, moderate relief, slightly weathered; 2, humid climate, low relief, moderately weathered; 4, intensely weathered

Fig. 11 Tectonic setting discrimination diagram for the Tipam sandstones: **a**, **b** Q_p–L_{vm}–L_{sm} Q_m–L_v–L_s triangular plots *after* Ingersoll and Suczek (1979); **c** SiO_2/Al_2O_3 versus K_2O/Na_2O bivariate plot *after* Roser and Korsch (1986), where, A1, continental island arc, A2, oceanic island arc; **d** SiO_2 versus (K_2O/Na_2O) bivariate plot *after* Murphy (2000)

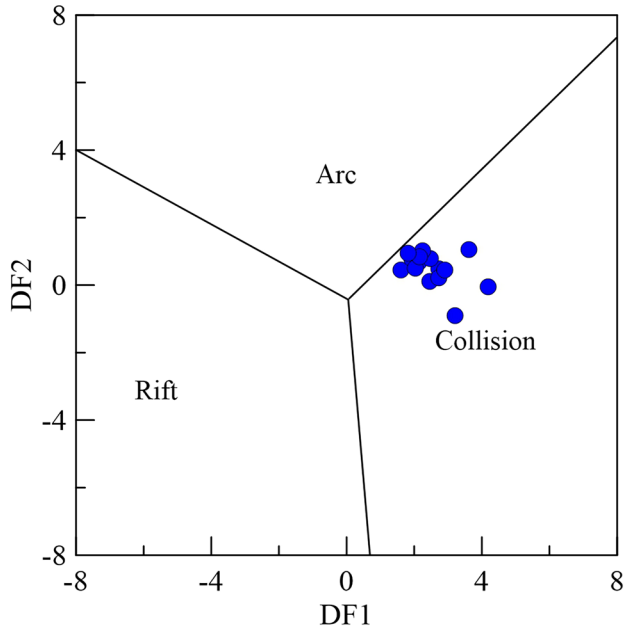

Fig. 12 Tectonic discriminant diagram of DF1 (Arc–Rift–Col)$_{m1}$ versus DF2 (Arc–Rift–Col)$_{m1}$ *after* Verma and Armstrong-Altrin (2013)

with the uplift of the Himalayas. The earlier-mentioned provenance analysis suggests that the Tipam Sandstone Formation has recycled sources. The reworked sediments from older passive margin deposits might have been mixed into the younger active margin sediments, resulting in mixed signals in the geochemical data. Furthermore, Verma and Armstrong-Altrin (2013) proposed a new model of the tectonic setting for the depositional basins by using the discriminant function of DF1 (Arc–Rift–Col)$_{m1}$ versus DF2 (Arc–Rift–Col)$_{m1}$, where the arc and collision fields represent the active margin, while the rift field indicates the passive margin setting. In this plot (Fig. 12), the studied samples are entirely plotted in the collision field, which implies an active margin tectonic setting for the Tipam sandstones.

6 Conclusions

The Tipam sandstones from the CTFB of the Bengal Basin display an average modal composition of $Q_{77}F_{11}L_{12}$, which classifies them as sublitharenite to lithic subarkose. The mineralogical behavior of the studied sandstones is consistent with the geochemical composition, characterized by higher concentrations of SiO_2, Al_2O_3, and Fe_2O_3, and lower values of TiO_2, MnO, CaO, MgO, Na_2O, and K_2O values. The abundance of feldspar and ductile grains, the negative correlation between Si_2O/Al_2O_3 and total quartz (Qt), and the higher ICV (> 1.0) values indicate that the Tipam sandstones are texturally and compositionally immature. The provenance discriminant diagrams suggest a recycled sedimentary provenance with dominance from felsic igneous sources. The weathering indices of CIA, PIA, and CIW, along with the triangular plots of A–CN–K, (A–K)–C–N, A–CNK–FM, and MFW, reflect a weak to moderate degree of chemical weathering under sub-humid climate conditions. The petrographic and geochemical results suggest that the Tipam sandstones were deposited in an active margin tectonic setting, with the majority of sediments originating from the Lesser Himalayan Sequence and a lesser portion from the Higher Himalayan Crystalline Sequence, Sub-Himalaya, and Indo-Burma Ranges during Pliocene period.

Acknowledgements The first author is grateful to the Faculty of Mathematical and Physical Sciences at Jahangirnagar University for their financial support during the fiscal year 2023–2024 for this project. We also appreciate the authority of IMMM of BCSIR at Joypurhat, Bangladesh, for providing access to their XRF laboratory, which was crucial for the successful completion of the experimental work.

Author contributions Author contributions are as follows: 1. Sayem, ASM—Planning, fieldwork, writing, and reviewing the main manuscript 2. Mondal, P—Thin section laboratory work, data analyses, and preparing all Figs. 3. Sah Alam, M—XRF laboratory work 4. Abdullah, R—Fieldwork, and reviewing manuscript 5. Rahman, MJJ—Reviewing the manuscript 6. Yeasmin, R—Field work.

Data availability No datasets were generated or analysed during the current study.

Declarations

Competing interests The authors declare that they have no known competing financial interests or personal relationships that could have appeared to influence the work reported in this paper. There are no conflict of interest to disclose.

References

Abdullah, R., Aurthy, M. R., Khanam, F., Hossain, M. M., & Sayem, A. S. M. (2022). Structural development and tectonostratigraphic evolution of the Sylhet Trough (northeastern Bengal Basin) in the context of Cenozoic Himalayan Orogeny: Insights from geophysical data interpretation. *Marine and Petroleum Geology, 138*, 105–544.

Abdullah, R., Hossain, M. S., Aktar, M. S., Hossain, M. M., & Khanam, F. (2021a). Structural initiation along the frontal fold-thrust system in the western Indo-Burman Range: Implications for the tectonostratigraphic evolution of the Hatia trough (Bengal Basin). *Interpretation, 9*(3), 1–25.

Abdullah, R., Sayem, A. S. M., Yeasmin, R., Rahman, M. M., Bari, Z., & Khanam, F. (2021b). Plio-Pleistocene to Recent Tectonostratigraphic evolution of the Lalmai Anticline in the western Indo-Burman Range (Bangladesh): Insights from lithofacies analysis and structural synthesis. *Arabian Journal of Geosciences, 14*(392), 1–11.

Alam, M., Curray, J. R., Chowdhury, M. L. R., & Gani, M. R. (2003). An overview ofthe sedimentary geology of the Bengal Basin about the regionaltectonic framework and basin-fill history. *Journal of Sedimentary Geology, 150*, 179–208.

Armstrong-Altrin, J. S., Lee, Y. I., Kasper-Zubillaga, J. J., & Trejo-Ramírez, E. (2017). Mineralogy and geochemistry of sands along the Manzanillo and El Carrizal beach areas, southern Mexico: implications for palaeoweathering, provenance, and tectonic setting. *Geological Journal, 52*(4), 559–582.

Armstrong-Altrin, J. S., Ramos-Vázquez, M. A., Hermenegildo-Ruiz, N. Y., & Madhavaraju, J. (2021). Microtexture and U-Pb geochronology of detrital zircon grains in the Chachalacas beach, Veracruz State, Gulf of Mexico. *Geological Journal, 56*(5), 2418–2438.

Basu, A. (1985). Reading provenance from detrital quartz. In G. G. Zuffa (Ed.), *Provenance of Arenites, D* (pp. 1–18). Reidel Publishing Company.

Bhatia, M. R. (1983). Plate tectonic and geochemical composition of sandstone. *Journal of Geology, 92*, 611–627.

Bhatia, M. R., & Crook, K. A. (1986). Trace element characteristics of graywackes and tectonic setting discrimination of sedimentary basins. *Contributions to Mineralogy and Petrology., 92*(2), 181–193.

Boggs, S. J. (2009). *Principles of sedimentology and stratigraphy* (3rd ed.). Prentice Hall.

Bracciali, L., Najman, Y., Parrish, R. R., Akhter, S. H., & Millar, I. (2015). The Brahmaputra tale of tectonics and erosion: Early Miocene River capture in the Eastern Himalaya. *Earth and Planetary Science Letters, 415*, 25–37.

Critelli, S., & Garzanti, E. (1994). Provenance of the Lower Tertiary Murree redbeds (Hazara-Kashmir Syntaxis, Pakistan) and initial rising of the Himalayas. *Sedimentary Geology, 89*(3–4), 265–284.

Cullers, R. L. (2000). The geochemistry of shales, siltstones and sandstones of Pennsylvanian-Permian age, Colorado, USA: Implications for provenance and metamorphic studies. *Lithos, 51*, 181–203.

Curray, J. R. (1991). Geological history of the Bengal geosyncline. *Journal of Association of Exploration Geophysicists, 12*(4), 209–219.

Davies, C., Best, J., & Collier, R. (2003). Sedimentology of the Bengal Shelf, Bangladesh: Comparison of late Miocene sediments, Sitakund anticline, with the modern, tidal dominated shelf. *Sedimentary Geology., 155*(3–4), 271–300.

Dickinson, W. R. (1985). Interpreting provenance relations from detrital modes of sandstones. In G. G. Zuffa (Ed.), *Provenance of arenites* (Vol. 148, pp. 333–361). NATO Advanced Study Institute Series.

Dickinson, W. R., & Suczek, C. A. (1979). Plate tectonics and sandstone compositions. *AAPG Bulletin, 63*(12), 2164–2182.

Dina, N. T., Rahman, M. J. J., Hossain, M. S., & Sayem, A. S. M. (2016). Provenance of the Neogene succession in the Bandarban structure, South-East Bengal Basin, Bangladesh: Insights from petrography and petrofacies. *Himalayan Geology, 37*, 141–152.

Fedo, C. M., Nesbitt, W. H., & Young, G. M. (1995). Unraveling the effects of potassium metasomatism in sedimentary rocks and paleosols, with implications for paleo weathering conditions and provenance. *Geology, 23*(10), 921–924.

Gani, M. R., & Alam, M. M. (2003). Sedimentation and basin-fill history of the Neogene clastic succession exposed in the southeastern fold belt of the Bengal Basin, Bangladesh: A high-resolution sequence stratigraphic approach. *Sedimentary Geology, 155*(30), 227–270.

Garzanti, E., & Andò, S. (2007). Plate tectonics and heavy mineral suites of modern sands. In M. A. Mange & D. T. Wright (Eds.), *Heavy minerals in use. Developments in sedimentology* (Vol. 58, pp. 741–763).

Garzanti, E., Baud, A., & Mascle, G. (1987). Sedimentary record of the northward flight of India and its collision with Eurasia (Ladakh Himalaya, India). *Geochimica Et Cosmochimica Acta, 1*, 297–312.

Goto, A., & Tatsumi, Y. (1994). Quantitative analysis of rock samples by an X-ray fluorescence spectrometer (I). *The Rigaku Journal, 11*, 40–59.

Goto, A., & Tatsumi, Y. (1996). Quantitative analysis of rock samples by an X-ray fluorescence spectrometer (II). *The Rigaku Journal, 13*, 20–38.

Harnois, L. (1988). The CIW index: A new chemical index of weathering. *Sedimentary Geology, 55*(3–4), 319–322.

Hayashi, K. I., Fujisawa, H., Holland, H. D., & Ohmoto, H. (1997). Geochemistry of ~1.9 Ga sedimentary rocks from northeastern Labrador, Canada. *Geochimica Et Cosmochimica Acta, 61*(19), 4115–4137.

He, Z., Guo, Z. T., Yang, F., Sayem, A. S. M., Wu, H., Zhang, Z., Hao, Q., Xiao, G., Han, L., Fu, Y., Wu, Z., & Hu, H. (2019). Provenance of Cenozoic sediments in the Xining Basin revealed by Nd and Pb isotopic evidence: Implications for tectonic uplift of the NE Tibetan Plateau. *Geochemistry, Geophysics, Geosystems, 20*(10), 4531–4544.

Herron, M. M. (1988). Geochemical classification of terrigenous sands and shale from core or log data. *Journal of Sedimentary Petrology, 58*, 820–829.

Hossain, H. M. Z. (2019). Major, trace, and REE geochemistry of the Meghna River sediments, Bangladesh: Constraints on weathering and provenance. *Geological Journal, 55*(5), 3321–3343.

Hossain, H. M. Z., Kawahata, H., Roser, B. P., Sampei, Y., Manaka, T., & Otani, S. (2017). Geochemical characteristics of modern river sediments in Myanmar and Thailand: Implications for provenance and weathering. *Chemie der Erde, 77*, 443–458.

Ingersoll, R. V., & Suczek, C. A. (1979). Petrology and provenance of Neogene sand from Nicobar and Bengal fans, DSDP sites 211 and 218. *Journal of Sedimentary Research, 49*(4), 1217–1228.

Johnson, S. Y., & Alam, A. M. N. (1991). Sedimentation and tectonics of the Sylhet trough, Bangladesh. *GSA Bulletin, 103*, 1513–1527.

Le Bas, M. J., Le Maitre, R. W., Streckeisen, A., & Zanettin, B. (1986). A chemical classification of volcanic rocks based on the total alkali-silica diagram. *Journal of Petrology, 27*, 745–750.

Li, L., Liu, Z., Sun, P., Li, Y., & George, S. C. (2020). Sedimentary basin evolution, gravity flows, volcanism, and their impacts on the formation of the Lower Cretaceous oil shales in the Chaoyang Basin, northeastern China. *Marine and Petroleum Geology, 119*, 104–472.

Long, X., Yuan, C., Sun, M., Xiao, W., Wang, Y., Cai, K., & Jiang, Y. (2012). Geochemistry and Nd isotopic composition of the Early Paleozoic flysch sequence in the Chinese Altai, Central Asia: Evidence for a northward-derived mafic source and insight into model ages in an accretionary orogen. *Gondwana Research, 22*, 554–566.

McBride, E. F. (1963). A classification of common sandstones. *Journal of Sedimentary Petrology, 33*, 664–669.

Murphy, J. B. (2000). Tectonic influence on sedimentation along the southern flank of the Late Paleozoic Magdalen Basin in the Canadian Appalachians: Geochemical and isotopic constraints on the Horton Group in the St. Marys Basin, Nova Scotia. *GSA Bulletin, 112*, 997–1011.

Najman, Y., Allen, R., Willett, E. A. F., et al. (2012). The record of Himalayan erosion preserved in the sedimentary rocks of the Hatia Trough of the Bengal Basin and the Chittagong Hill Tracts, Bangladesh. *Basin Research, 24*(5), 499–519.

Najman, Y., Bickle, M., BouDagher-Fadel, M. K., et al. (2008). The Paleogene record of Himalayan erosion: Bengal Basin, Bangladesh. *Earth and Planetary Science Letters, 273*(1–2), 1–14.

Nesbitt, H. W., & Young, G. M. (1982). Early Proterozoic climates and plate motions inferred from major element chemistry of lutites. *Nature, 299*(5885), 715–717.

Nesbitt, H. W., & Young, G. (1984). Prediction of some weathering trends of plutonic and volcanic rocks based on thermodynamic

and kinetic considerations. *Geochimica Et Cosmochimica Acta, 48*(7), 1523–1534.

Noa Tang, S. D., Ntsama Atangana, J., & Onana, V. L. (2020). Mineralogy and geochemistry of alluvial sediments from the Kadey plain, eastern Cameroon: Implications for provenance, weathering, and tectonic setting. *Journal of African Earth Sciences, 163*, 103763.

Ohta, T., & Arai, H. (2007). Statistical empirical index of chemical weathering in igneous rocks: A new tool for evaluating the degree of weathering. *Chemical Geology, 240*(3), 280–297.

Pettijohn, F. J., Potter, P. E., & Siever, R. (1972). Sand and sandstone. Plate motions inferred from major element chemistry of lutites. *Precambrian Research, 147*, 124–147.

Potter, P. E. (1978). Petrology and chemistry of modern big river sands. *The Journal of Geology, 86*(4), 423–449.

Rahman, M. J. J., & Faulp, P. (2003). The composition of the subsurface Neogene shales of the Surma Group from the Sylhet Trough, Bengal Basin, Bangladesh. *Sedimentary Geology, 155*(3), 407–417.

Rahman, M. J. J., Sayem, A. S. M., & Bhuiyan, M. H. (2014a). Geochemistry of the Plio-Pleistocene Dupi Tila sandstones from the Surma Basin, Bangladesh: Implications for provenance, tectonic setting and weathering. *Himalayan Geology, 35*(2), 162–170.

Rahman, M. J. J., Sayem, A. S. M., & McCann, T. (2014b). Geochemistry and provenance of the Miocene Sandstones of the Surma Group from the Sitapahar Anticline, southeastern Bengal Basin, Bangladesh. *Journal Geological Society of India, 83*, 447–456.

Rahman, M. J. J., Xiao, W., Hossain, M. S., Yesmin, R., Sayem, A. S. M., Ao, S., Yang, L., Abdullah, R., & Dina, N. T. (2020). Geochemistry and detrital zircon U-Pb dating of Pliocene-Pleistocene sandstones of the Chittagong Tripura Fold Belt (Bangladesh): Implications for provenance. *Gondwana Research, 78*, 278–290.

Reimann, K. U. (1993). *Geology of Bangladesh* (1st ed.). Borntraeger.

Roser, B. P., & Korsch, R. J. (1986). Determination of tectonic setting of sandstone-mudstone suites using SiO_2 content and K_2O/Na_2O ratio. *The Journal of Geology, 94*(5), 635–650.

Roser, B. P., & Korsch, R. J. (1988). Provenance signatures of sandstone-mudstone suites determined using discrimination function analysis of major element data. *Chemical Geology, 67*, 119–139.

Sayem, A. S. M., Guo, Z. T., Wu, H., Zhang, C., Yang, F., Xiao, G., & He, Z. (2018). Sedimentary and geochemical evidence of Eocene climate change in the Xining Basin, northeastern Tibetan Plateau. *Science China: Earth Sciences, 61*(9), 1292–1305.

Sayem, A. S. M., & Rahman, M. J. J. (2012). Sandstone petrography of the Surma Group succession exposed in the Sitapahar Anticline, Bengal Basin, Bangladesh. *Bangladesh Geoscience Journal, 18*, 23–41.

Sayem, A. S. M., Rahman, M. J. J., Abdullah, R., & Azim, K. M. R. (2022). Diagenetic history of the Miocene Surma Group sandstones from the Eastern Fold Belt of the Bengal Basin. *Journal of Asian Earth Sciences X, 7*, 100098.

Sayem, A. S. M., Rokonuzzaman, M., Shahriar, M. S., Abdullah, R., Bari, Z., & Hossen, M. S. (2023). Major and trace element geochemistry of the Atrai River sediments from the Bengal Basin (Bangladesh): Implication for provenance, chemical weathering, and tectonic setting in the southeastern Himalaya. *Arabian Journal of Geosciences, 16*, 487.

Searle, M. P., Noble, S. R., Hurford, A. J., & Rex, D. C. (1999). Age of crustal melting, emplacement and exhumation history of Shivling leucogranite, Garhwal Himalaya. *Geological Magazine, 136*(5), 513–525.

Shamsuddin, A. H. M., & Abdullah, S. K. M. (1997). Geologic evolution of the Bengal Basin and its implication in petroleum exploration in Bangladesh. *Indian Journal of Geology, 69*, 93–121.

Singh, P. (2010). Geochemistry and provenance of stream sediments of the Ganga River and its major tributaries in the Himalayan region of India. *Chemical Geology, 269*(3–4), 220–236.

Suttner, L. J., & Dutta, P. K. (1986). Alluvial sandstone composition and paleoclimate framework mineralogy. *Journal of Sedimentary Petrology, 56*, 329–345.

Taylor, S. R., & McLennan, S. M. (1985). *The continental crust: Its composition and evolution. An examination of the geochemical record preserved in sedimentary rocks*. Oxford: Blackwell Science.

Uddin, A., & Lundberg, N. (1998). Cenozoic history of the Himalayan Bengal system: Sand composition in the Bengal Basin, Bangladesh. *GSA Bulletin, 110*(4), 497–511.

Verma, S. P., & Armstrong-Altrin, J. S. (2013). New multi-dimensional diagrams for tectonic discrimination of siliciclastic sediments and their application to Precambrian basins. *Chemical Geology, 355*, 117–180.

Weltje, G. J., Meijer, X. D., & Doer, P. L. (1998). Stratigraphic inversion of siliciclastic Basin fills: A note on the distinction between supply signals resulting from tectonic and climate forcing. *Basin Research, 10*, 129–153.

Wronkiewicz, D. J., & Condie, K. C. (1987). Geochemistry of Archean shales from the Witwatersrand Supergroup, South Africa: Source-area weathering and provenance. *Geochimica Et Cosmochimica Acta, 51*, 2401–2416.

Yang, L., Xiao, W. J., Rahman, M. J. J., et al. (2020). Indo-Burma passive amalgamation along the Kaladan Fault: Insights from zircon provenance in the Chittagong-Tripura Fold Belt (Bangladesh). *Geological Society of America Bulletin, 132*(9–10), 1953–1968.

Yang, L., Xiao, W., Rahman, M. J. J., Windley, B. F., Schulmann, K., Songjian, A., Chen, Z., & Li, R. (2019). Provenance of the Cenozoic Bengal Basin sediments: Insights from UePb ages and Hf isotopes of detrital zircons. *Geological Journal, 54*, 978–990.

Yeasmin, R., Abdullah, R., Hossain, M. S., et al. (2024). Petrography, geochemistry, and detrital zircon U-Pb dating of the Pliocene-Pleistocene Dupi Tila Formation from the Lalmai Anticline, Bengal Basin: Regional tectonic implications. *Geological Journal, 59*, 1239–1261.